VALIDATION OF 3D HELIOSEISMIC INVERSIONS OF TRAVEL-TIMES THROUGH SIMULATIONS OF ARTIFICIAL DATA WITH THE CORRECT NOISE STATISTICS

Sébastien Couvidat, Laurent Gizon, and Aaron C. Birch

W.W. Hansen Experimental Physics Laboratory, Stanford University, Stanford, CA 94305-4085, USA

ABSTRACT

In time-distance helioseismology most inversion procedures ignore the correlations in the data errors, which may be large as shown by Gizon & Birch (2004). Here we simulate the travel-time perturbations that result from a known distribution of sound-speed inhomogeneities (simulating sunspot-like structures) using wave-based sensitivity kernels. A realistic stochastic noise component is added to the data. We then apply a 3D inversion procedure that takes into account the full covariance matrix of the simulated data. The validation of the inversion is achieved through comparison of the inferred sound-speed distribution with the exact solution.

Key words: time-distance helioseismology; 3D inversion; noise covariance.

1. TIME-DISTANCE SEISMOLOGY

Time-Distance Helioseismology (Duvall et al. 1993) gives us access to local properties of the plasma below the visible surface of the Sun. It is based on the travel-time perturbations of wavepackets, due to their interaction with inhomogeneities of the solar plasma. These travel-time perturbations are obtained through temporal cross-covariances of Doppler velocities $\phi(\mathbf{r},t)$ at different locations $\mathbf{r}=(x,y)$ on the solar surface. These cross-covariances are averaged over annuli centered at $\mathbf{r}$ and of mean radius Δ. Here we only work with p modes and the perturbations $\delta\tau_{mn}(\mathbf{r},\Delta)$ in their mean travel-times $\tau_{mn}(\mathbf{r},\Delta)$ relative to travel times averaged over a quiet Sun region. These τ_{mn} are the averages of "in" and "out" travel-times (for wave propagating from/to the central point $\mathbf{r}$ to/from the annulus of mean radius Δ). These $\delta\tau_{mn}$ are in first approximation related to the sound-speed perturbations through:

$$\delta\tau_{mn}(\mathbf{r},\Delta)=\iiint K^{\Delta}_{mn}(\mathbf{r}-\mathbf{r}',z)\frac{\delta c}{c}(\mathbf{r}',z)\mathbf{dr}'dz \quad (1)$$

Where K^{Δ}_{mn} is a sensitivity kernel for sound-speed perturbations, and $\delta c/c$ is a relative sound-speed difference. Our goal is to invert the sound speed by fully taking into account the noise statistics on the $\delta\tau_{mn}$ data. This has never been done before in local helioseismology. We need to compute the full travel-time noise covariance and use it in the inversion process.

2. ARTIFICIAL DATACUBES

We use data from the MDI/SoHO experiment (Scherrer et al. 1995): those are time series of high-resolution dopplergrams obtained in May 2001 at a cadence of 1 min and centered on a quiet Sun region. The sixteen $150\times150\times128$ grid-nodes datacubes were combined into four consecutive datacubes of time length 512 min. We computed the four corresponding 3D power spectra $P(k_x,k_y,\omega)$ and averaged them. We then made the resulting power spectrum isotropic by averaging it over $k=(k_x^2+k_y^2)^{\frac{1}{2}}$, to obtain the expectation value of the solar oscillations power spectrum $P(k,\omega)$ (Fig. 1). To obtain the travel-time noise statistics, we produce artificial datacubes in the Fourier domain: $\phi(\mathbf{k},\omega)=P(k,\omega)^{\frac{1}{2}}\mathcal{N}(\mathbf{k},\omega)$. $\mathcal{N}(\mathbf{k},\omega)$ is a complex Gaussian random variable with independent real and imaginary parts, zero mean, and unit standard deviation. In the space domain the spatial sampling of these datacubes $\phi(\mathbf{r},t)$ is 1.652 Mm. We generated 300 realizations of such datacubes.

3. TEMPORAL CROSS-COVARIANCES

We want travel-time perturbation maps for eleven distances Δ. Table 1 lists these distances and the corresponding phase-speed Gaussian filters. These Δ values were used by Kosovichev, Duvall, & Scherrer (2000) to study an active region. Each realization $\phi(\mathbf{k},\omega)$ is multiplied by Gaussian phase-speed filters $F(k,\omega)$: we only keep the power corresponding to specific horizontal phase-speeds (Fig. 1). This way we only retain waves that propagate along a similar ray-path, and we reduce the noise level on the temporal cross-covariances. We compute these temporal point-to-annulus cross-covariance functions $\bar{C}(\mathbf{r},\Delta,t)$, following Gizon & Birch (2004) (see Fig. 2):

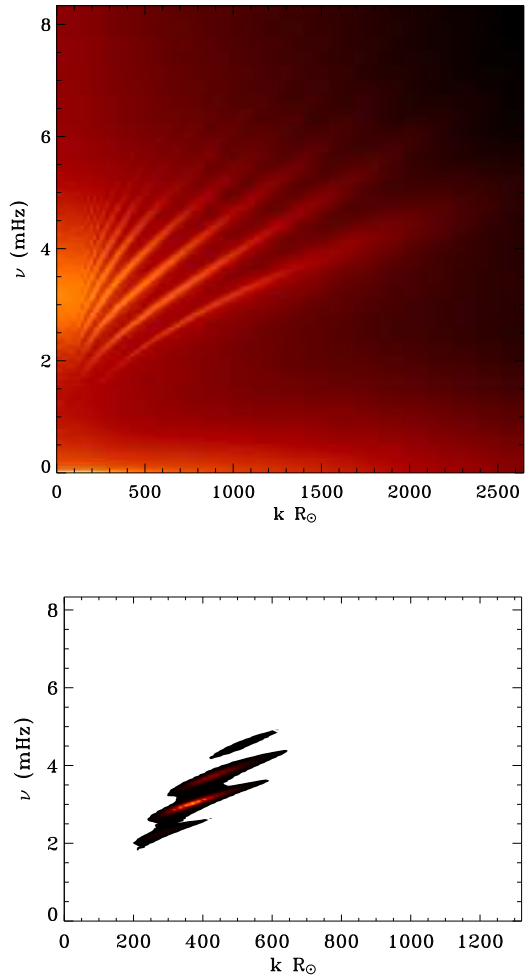

Figure 1. Upper panel: power spectrum $P(k, \nu = \frac{\omega}{2\pi})$ obtained with MDI high-resolution data. This spectrum is used as the expectation value of the solar oscillations power spectrum. Lower panel: example of filtered power spectrum of a datacube realization. The Gaussian phase-speed filter applied here keeps waves with a phase speed $\omega/k \approx 35.5$ km s^{-1}. We also applied a filter to remove the f-mode ridge.

$$\bar{C}(\mathbf{r}, \Delta, t) = \frac{\sum_{\mathbf{r_1}} \aleph(|\mathbf{r_1} - \mathbf{r}| - \Delta)\, C(\mathbf{r}, \mathbf{r_1}, t)}{\sum_{\mathbf{r}'} \aleph(|\mathbf{r}' - \mathbf{r}| - \Delta)} \quad (2)$$

Where the temporal point-to-point cross-covariance function is defined as:

$$C(\mathbf{r}, \mathbf{r_1}, t) = \frac{h_t}{T - |t_j|} \sum_i \phi(\mathbf{r}, t_i)\phi(\mathbf{r_1}, t_i + t_j) \quad (3)$$

$\aleph(x)$ is a window function ($\aleph(x) = 1$ if $|x| <$width(Δ)), $T = 512$ min, and h_t is the time sampling (1 min). Our datacubes contain 150×150 grid nodes in the (x, y)-plane. We compute $\bar{C}(\mathbf{r}, \Delta, t)$ for the eleven Δ values and for the nodes for which the largest annulus fits entirely within the (x, y)-grid. By averaging the $\bar{C}(\mathbf{r}, \Delta, t)$ over all these nodes, we produce a reference cross-covariance function $\bar{C}_{ref}(\Delta, t)$.

Table 1. Distances Δ used to derive the travel-time perturbation ($\delta\tau_{mn}$) maps, and corresponding parameters for the Gaussian phase-speed filters: mean phase speed and dispersion (courtesy of T. L. Duvall). The Gaussian filters are written as $F(k, \omega) = \exp\left(-(\frac{\omega}{k} - v_0)^2 / 2\delta v_0^2\right)$. We multiply $\phi(\mathbf{k}, \omega)$ by $\sqrt{F}$.

Annulus #	Δ (Mm)	v_0 (km s^{-1})	δv_0 (km s^{-1})
1	4.13-8.26	12.77	4.37
2	6.61-10.74	14.87	4.37
3	9.21-14.04	17.49	4.37
4	14.87-19.00	25.82	6.43
5	19.82-28.91	35.46	8.74
6	26.43-34.69	39.71	5.07
7	32.21-41.30	43.29	5.25
8	38.82-47.08	47.67	5.95
9	44.61-53.69	52.26	7.43
10	51.21-59.47	57.16	6.30
11	57.00-65.26	61.13	5.68

4. TRAVEL-TIMES COMPUTATION

Once we have the temporal cross-covariances for the appropriate (x, y) pairs of a datacube realization, we derive the travel-time perturbations $\delta\tau_{mn}(\mathbf{r}, \Delta)$ related to the reference cross-covariance. We apply Eqs. (3) and (4) of Gizon & Birch (2004). Fig. 3 shows an average of the power spectra of the resulting travel-time maps over the 300 artificial datacube realizations. We use these 300 realizations of eleven travel-time maps to compute the travel-time noise covariance matrices.

5. FORWARD & INVERSE PROBLEMS

To examine the effects of noise statistics on the sound-speed inversions, we compare inversions of artificial travel-time perturbation maps done with and without accounting for this noise statistics. The artificial travel-time datamaps are obtained through the forward problem using Born kernels (Birch, Kosovichev, & Duvall 2004). These kernels take into account the sensitivity of wavepackets to $\delta c/c$ perturbations off the ray-paths. We apply these kernels on a $\delta c/c$ slab simulating sunspot-like structures (see Couvidat et al. 2004). We then add a travel-time noise realization to the resulting $\delta\tau_{mn}(\mathbf{r}, \Delta)$ maps, and invert them using the same Born kernels. The noise standard deviation on the different travel-time maps ranges from $\sigma = 8$ to $\sigma = 18$ s. The inversion is done with a regularized least-squares method through the multi-channel de-

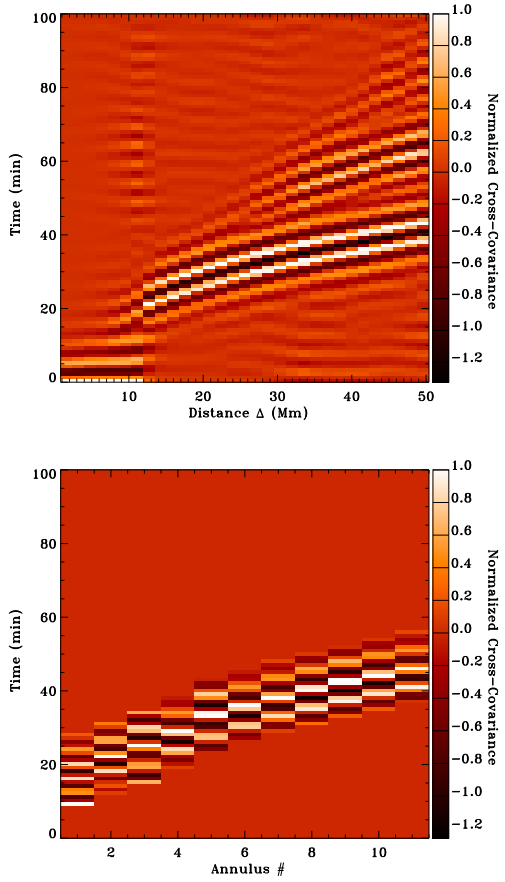

Figure 2. Example of temporal cross-covariance functions. Upper panel: obtained for 31 distances Δ, no phase-speed filter, and f modes removed. Lower panel: obtained for the eleven distances Δ listed in Table 1. This is the actual reference cross-covariance $\bar{C}_{ref}(\Delta, t)$ used in this paper for the travel-time computations. A specific phase-speed filter was applied for each Δ value, on top of the f-mode filter. We show only the first-bounce ridge. In both panels the covariances were normalized.

convolution (MCD) algorithm (see Jensen, Jacobsen, & Christensen-Dalsgaard 1998). The MCD is based on the translational invariance of the sensitivity kernels. Thus Eq. 1 amounts to a convolution product in the (x, y)-plane. In the Fourier domain, this convolution product is a basic multiplication. Therefore we invert the travel-time perturbation maps in the (k_x, k_y)-plane. Instead of inverting a huge 3D problem, we invert lots of 1D problems (in the z direction): one for each (k_x, k_y) pair. We regularize the solution by its norm weighted by the inverse of the sound speed at each z layer.

Using our 300 realizations of artificial maps of travel-time noise, we can compute the noise covariance matrices $\mathrm{Cov}(\mathbf{k}, \Delta, \Delta')$. Actually we expect these covariance matrices to depend only on k. Also we average the different matrices over k and obtain 11×11 matrices $\mathrm{Cov}(k, \Delta, \Delta')$ that give the covariance at a given horizontal wavenumber of the travel-time noise $\delta\tau_{mn}(\mathbf{k}, \Delta)$ obtained for different annulus radii. To use them in the inversion process, we write each matrix as

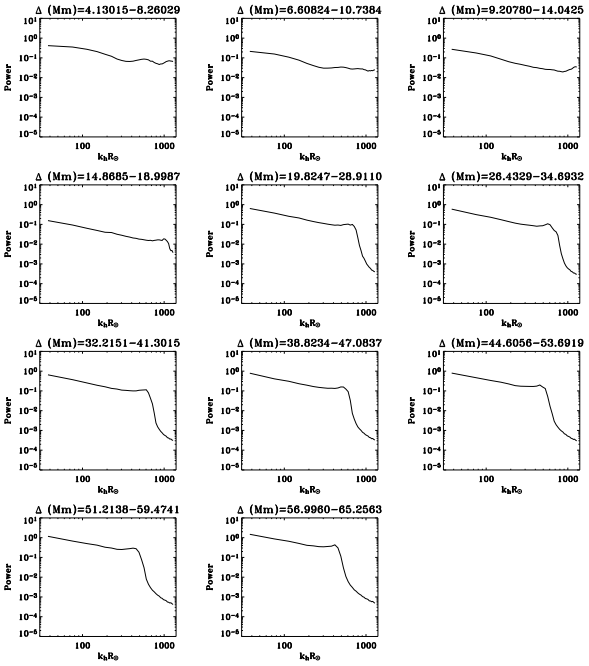

Figure 3. Power spectra of the travel-time perturbation $\delta\tau_{mn}(\mathbf{r}, \Delta)$ maps (azimuthal average). These power spectra are close to those shown in Jensen, Duvall, & Jacobsen (2003), and Gizon & Birch (2004).

$\mathrm{Cov}(k, \Delta, \Delta') = LL^T$, where L is a lower triangular matrix (Cholesky decomposition), and scale the kernel and data matrices by L^{-1} (Hansen 1997).

6. PRELIMINARY RESULTS

For information we show the travel-time noise correlation matrix $\mathrm{Corr}(\mathbf{r} - \mathbf{r}' = 0, \Delta, \Delta')$ (Fig. 4) obtained by horizontal averaging. $\mathrm{Corr}(0, \Delta, \Delta')$ is a 11×11 matrix that gives the different correlation values for travel times $\delta\tau_{mn}(\mathbf{r}, \Delta)$ derived with annuli of mean radii Δ and Δ'. $\mathrm{Corr}(0, \Delta, \Delta')$ is not actually used in the inversion process since we work in the Fourier domain. As expected the noise correlation is larger for travel-times obtained for two annuli that overlap.

We invert two sets of artificial travel-time datamaps. Figs. 5 & 6 show vertical cuts in the inversion results. These preliminary results are only based on a single inversion (i.e. inversion of artificial data "polluted" by a single noise realization). Therefore it is difficult to draw any firm conclusion, which would require inversions of a large number of datamaps with the same data but a different travel-time noise realization. However, it seems that taking into account the noise statistics in the inversion process slightly reduces the noise level on the results, especially for small-scale structures (like the ones on Fig. 6): the signal-to-noise ratio seems improved. If so, this should help us in better inverting fine physical details. Here the correlations on the travel times are not very large due to our specific choice of Δ distances and phase-speed filters. Therefore we do not expect a dramatic impact on the inversion results. Taking into account these

correlations is not computationally expensive and does not reduce the performance of the inversion process, even though the computation of the correlations themselves is a slow process.

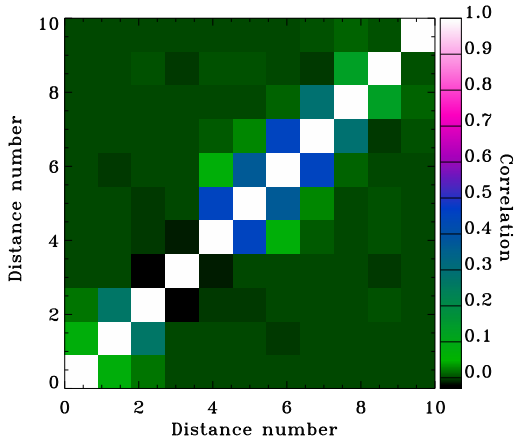

Figure 4. Correlation matrix $\mathrm{Corr}(0, \Delta, \Delta')$ *obtained for the 11 distances* Δ *listed in Table 1. Each pixel gives the correlation between travel times computed for an annulus of radius* Δ *and one of radius* Δ'*. Correlation is low off the diagonal for two reasons: (1) annuli do not strongly overlap (2) phase-speed filters are different. Therefore the wavepackets used to compute the cross-covariance at different* Δ *values are not the same.*

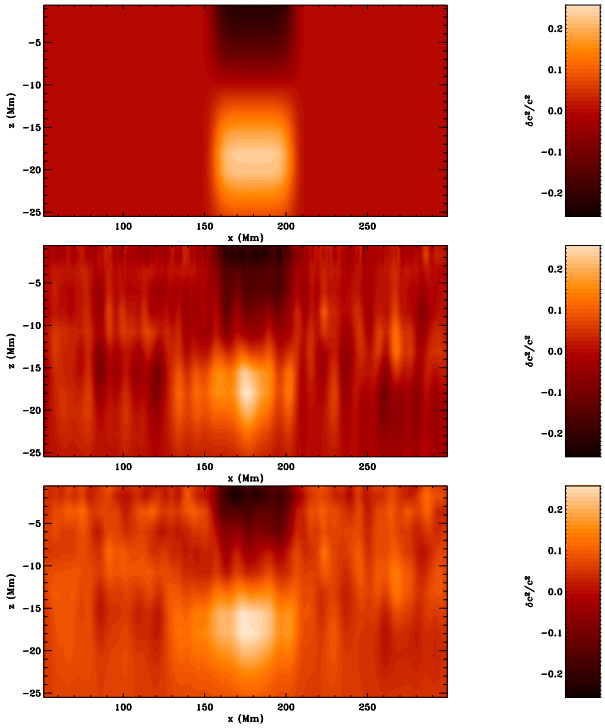

Figure 5. Vertical cuts in the inversion results for the first artificial dataset (a large-scale structure). The upper panel shows the exact solution. Noise is added with a dispersion equal to the one obtained after 8 hours and a half of observation. Middle panel: inversion without taking into account the noise covariance matrices. Lower panel: inversion with the noise covariance matrices.

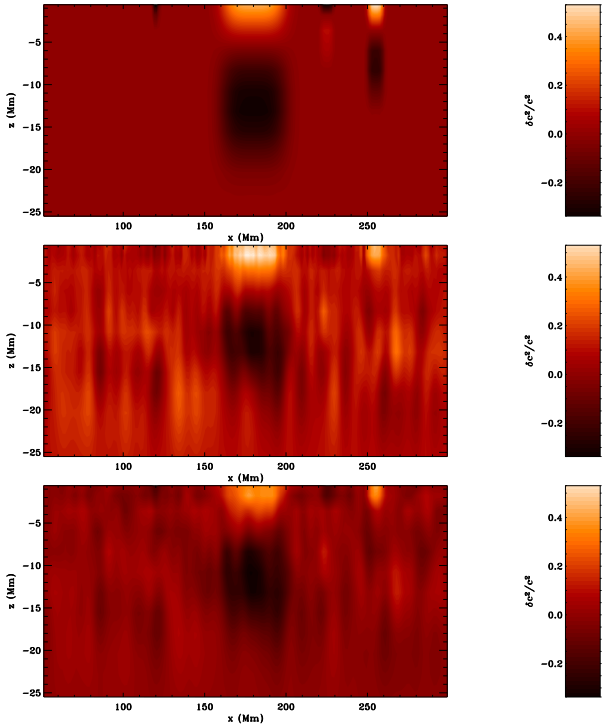

Figure 6. Same as Fig. 5 but for the second artificial dataset (simulating four small-scale structures).

ACKNOWLEDGMENTS

This work was supported by NASA grants NAG5-13261 and NAG5-12452

REFERENCES

1. Birch, A. C., Kosovichev, A. G., & Duvall, T. L., Jr. 2004, ApJ, 608, 580
2. Couvidat, S., Birch, A. C., Kosovichev, A. G., & Zhao, J. 2004, ApJ, 607, 554
3. Duvall, T. L., Jr., Jefferies, S. M., Harvey, J. W., & Pomerantz, M. A. 1993, Nature, 362, 430
4. Gizon, L., & Birch, A. C. 2004, ApJ, *accepted*
5. Hansen, P. C. 1997, in "Rank Defi cient and Discrete Ill-Posed Problems", SIAM Publications
6. Jensen, J. M., Jacobsen, B. H., & Christensen-Dalsgaard, J. 1998, proceedings of the SoHO 6/GONG 98 Workshop, ESA publications, 635
7. Jensen, J. M., Duvall, T. L., Jr., & Jacobsen, B. H. 2003, proceedings of the SoHO 12/GONG+ 2002 Workshop, ESA publications, 315
8. Kosovichev, A. G., Duvall, T. L., Jr., & Scherrer, P. H. 2000, Solar Physics, 192
9. Scherrer, P. H., et al. 1995, Solar Physics, 162, 129